Cosmic Radiation Reliability Analysis for Aircraft Power Electronics

Mikhail Dobynde*, Jayakrishnan Harikumaran*, Jingnan Guo, Patrick Wheeler, *Fellow, IEEE*, Michael Galea, *Senior Member, IEEE*, Giampaolo Buticchi, *Senior Member, IEEE*

***Abstract*—Cosmic Ray induced failures are a major concern for the electronic system reliability of airborne and space systems. Power system voltages on aerospace platforms are on a steady upward trend. High voltage power converters suffer from Single Event Burnout failures caused by cosmic rays. The established standards propose a scaling factor based on measured background galactic cosmic rays intensity at operating altitude to apply de-rating factors. The radiation environment in the atmosphere can be increased due to the cascading of primary solar energetic particles during solar eruptions. In this work, the altitude profile of the radiation environment is simulated using a GEANT4 Monte-Carlo code. The failure rates due to both background Galactic Cosmic Rays and Solar Energetic Particles are quantitatively evaluated. Further to the known influence of geomagnetic shielding of the cosmic rays, the geographical distribution of cosmic rays at flight altitude of 10 km are also presented. The estimated cosmic ray intensity is combined with experimentally measured failure rate to predict the impact on the reliability of power converters, giving a new level of accuracy in the modeling of such failure mode in more electric aircraft applications. It is shown for the first time in the scientific literature by using experimental data and state-of-the-art models, that the solar energetic particles storms fluxes vastly exceed the recommended standard and constitute a risk for the power electronics reliability.**

***Index Terms*—Cosmic rays, Power electronics, Reliability.**

NOMENCLATURE

AEA	All electric aircraft
BVR	Blocking voltage ratio
CR	Cosmic Ray
FIT	Failure in time
GCR	Galactic Cosmic Ray
MEA	More electric aircraft
RBD	Reliability block diagram
SEB	Single event burnout
SEE	Single event error
SEP	Solar energetic particle
3L-NPC	Three Level Neutral Point Clamped

I. INTRODUCTION

AVIATION industry is increasingly electrifying aircraft subsystems. The transition to ”More Electric Aircraft - MEA” and ”All Electric Aircraft - AEA” manifest as higher on board electrical power generation [1]. Electrical driven systems are expected to replace conventional mechanical systems - hydraulic actuators, instrument air system and even propulsion [2]. De-carbonisation, efficiency improvement, system simplification etc. are some of the key drivers for this trend [1].

The impact of Cosmic Rays (CRs) on avionics and space systems originally drew the attention of system designers to mitigate the potential radiation risks induced by CRs [3]. The most important components of CRs in the atmosphere of Earth are Galactic CRs (GCRs) and Solar Energetic Particles (SEPs) and secondary particle, which are induced by them in the atmosphere of the Earth. GCRs are low-intensity background fluxes of high-energy charged particles coming from the interstellar medium. GCRs in the inner heliosphere include about 2% electrons and 98% fully ionized atoms of different elements, mostly hydrogen (87%) and helium (12%) ions [4]. The GCR intensity is modulated by the heliospheric magnetic fields and thus varies with the 11-year solar activity cycle [5]. During periods of solar activity maximum, the GCR intensity is more depressed and vice verse. On the other hand, SEPs are high-intensity fluxes of particles (mainly protons and electrons) associated with sporadic solar eruptions such as solar flares and shocks driven by corona mass ejections [6]. Therefore, they are more frequent and more intensive during solar maximum periods.

In low voltage electronics, CR predominantly results in failures associated with Single Event Error (SEE), which is observable as bit errors in memory modules [7]. The mechanisms and the mitigation measures are well understood for low voltage systems, and often involve particular layout of the integrated circuits and shielding.

Alternatively, in high voltage power semiconductors, the failure mechanism due to CR is primarily due to single event burnout (SEB). The mechanism is outlined in [8]. The high energy particles, including both primary CRs and the secondary particles generated by the interactions of primary CR with the atmospheric molecules, may undergo nuclear and atomic interactions with semiconductor atoms and results in a charge in the semiconductor bulk. This charge is able to activate

M. Dobynde and J. Harikumaran contributed equally to this work.

This work is supported by the Strategic Priority Program of the Chinese Academy of Sciences (Grant No. XDB41000000), Natural Science Foundation of China (52250610219, 42074222, 42188101), and by Ministry of Science & Technology under National Key R&D Program of China, under Grant 2021YFE0108600 and by Ningbo Science and Technology Bureau under S&T Innovation 2025 Major Special Programme with grant No. of 2019B10071.

M. Dobynde and J. Guo are with the Deep Space Exploration Laboratory/School of Earth and Space Sciences, University of Science and Technology of China (USTC), Hefei, China. (e-mails: mikhail.dobynde@ustc.edu.cn; jnguo@ustc.edu.cn). J.Harikumaran and Pat Wheeler are with the Power Electronics, Machines and Control (PEMC) group, University of Nottingham, Nottingham, NG72RD, UK (e-mails: Jayakrishnan.Harikumaran@nottingham.ac.uk; Pat.Wheeler@nottingham.ac.uk). M. Galea is with the University of Malta (e-mail: michael.d.galea@um.edu.mt). G. Buticchi is with the Key Laboratory of More Electric Aircraft Technology of Zhejiang Province and with the Nottingham Ningbo China Beacons of Excellence Research and Innovation Institute, University of Nottingham Ningbo China, Ningbo 315100, China (e-mail: giampaolo.buticchi@nottingham.edu.cn).

parasitic elements in the semiconductor or simply generate a local high electric field zone. Energized particles in the local high electric field zone or in the activated parasitic element create a short circuit in the semiconductor during an expected blocking mode. In power converters, this unanticipated turn-on results in a shoot-through failure as a short circuit develops across the DC link [9].

The consequence of CR-induced failures is considered as critical for high-reliability systems on the ground, e.g., wafer processing machines [10]. For aerospace applications, the operating conditions are more exposed to CR radiation and the need for reliability is certainly much higher. International Electrotechnical Commission (IEC) standard [7] specifies the calculation method to estimate CR-induced failure in airborne systems. The IEC standard provides a scaling factor for latitude and altitude dependent CR failure rate estimation. Since the CR are dependent not only on the altitude, but also on the location on Earth, the solar cycles and solar events, this study aims to fill the gap of the existing literature and standard, by performing a thorough physics-based evaluation of the CR flux and estimating its effect on the failure rate of the power electronics on-board a more electric aircraft. A starter/generator application is taken as a study case. It is worth noting that, given the size of the power electronics systems, shielding may incur in unacceptable weight gain and consequent loss of economic benefits. This is especially true considering the actual electrification trend which is pushing towards the complete electrification of the propulsion systems with consequent increase of the volume of the onboard power electronics .

The main approach of this work is the validation of atmospheric radiation levels used for CR-induced failure calculations for aerospace power converters. To do so, we utilize the Radiation Environment and Dose on Earth – "REDEarth" [11] model to predict the radiation environment created by GCRs and SEPs at various altitudes in Earth's atmosphere. The model accounts for the geomagnetic cutoff as effective vertical geomagnetic cut-off rigidity (EVGCR) to predict the radiation flux intensity and spectra at different geographical locations, where CR failure rate is estimated by scaling the failure rate measured at reference radiation flux intensity. We compare the results against the radiation figure provided by the IEC standard for CR-induced failure rate estimation. Radiation levels during some solar events are found to be of significant concern as the number of SEB inducing particles are high during solar events. Hence mitigation measures such as voltage reduction or thermal control [12] are necessary against solar events. The impact of voltage variation on the converter sub-components are evaluated and presented with a case study.

This study makes a big step in advancing the understanding of the radiation impact on aircraft electronics at cruise altitude especially during solar events. Considering the increasing penetration of power electronics in aircraft application, this enables accurate controls in order to mitigate the failure rate to specific values without over-engineering the system (which would imply additional weight and therefore cost of operation).

The rest of the article is organized as follows: Section II presents the atmospheric radiation model validated against experimental data and applied to measured SEP spectra; section III describes how to predict CR-induced failure in power electronics; section IV presents the starter/generator case study and section V draws the conclusion.

II. Atmospheric radiation modelling

Estimation of CR-induced failures requires information on the radiation environment. The IEC standard 62396-4 was developed to provide a baseline radiation profile for SEB estimation of high voltage power devices for aircraft applications [7]. The IEC standard specifies that neutron flux density at any point in the atmosphere could be obtained by scaling the value given at a reference location specified by its latitude, longitude and altitude. The reference location from IEC 62396 is at 45°latitude and an altitude of 40000 ft. The reference neutron flux of 6000 cm^{-2} h^{-1} for neutrons with energy > 10 MeV is specified by the standard based on [13], [14] to evaluate SEB failure rate.

More accurate information on radiation dose rates is available from particle simulation software which has been validated against radiation measurements in the atmosphere. For instance, the Nowcast of Aerospace Ionizing Radiation System (NAIRAS) predicts atmospheric radiation exposure from GCRs and SEPs for aviation systems [15]. (http://sol.spacenvironment.net/~nairas/). However, the NAIRAS does not provide information about energy and angular spectrum of different types radiation particles.

A. Radiation environment profile

The REDEarth radiation model [11] provides detailed secondary particle flux profiles based on many parameters such as altitude, EVGCR, particle type, energy, and direction. The model is built using the response function approach [16], [17], i.e. for each CR particle, characterized with type, energy, and angle of incidence on the top of the atmosphere the model provides resulting radiation environment, characterized with particles' type, energy, angle, and altitude. The response functions are calculated by modeling particle propagation in the atmosphere with GEANT4 Monte-Carlo code [18]. The physical processes are described with the built-in physics list FTFP_BERT_HP. It uses the Fritiof model to simulate particles with energy above 10 GeV, Bertini cascade model for particles with energy below 10 GeV and High Precision neutron model to cover energy range below 20 MeV. The atmosphere is described as a set of 1000 concentric spherical layers each with the thickness of 100 m. The air density in each layer is set uniform and equal to the average density in this layer following the US standard atmosphere model [19]. The impinging zenith angle of CR particles on top of the atmosphere is divided into 10 bins of 10 degree-width except the innermost and outermost ones, which are 5 degrees each. These angular bins are used when calculating incoming CR spectrum for a specific EVGCR value.

We then use the REDEarth model to assess radiation profile from 32 large solar events [20] and GCRs during solar maximum and minimum. The Badhwar-O'Neill (BON) 2014

GCR model [21] has been used to describe primary GCR particle spectra. The model considers the transport of GCRs from the local interstellar medium to Earth's vicinity during different time of the solar activity cycle (that is normally characterized by the sunspot number). The modeled spectra are validated by comparing with available observations at the measured energy ranges. The intensity of GCR is modulated by the heliospheric magnetic field which evolves following the 11-year solar cycle. Fig.1 shows two GCR proton spectra for the beginning of 2003 that is the solar maximum of solar cycle 23 (with monthly sunspot number of 133.5) and for the the middle of 2019, i.e., the solar minimum in solar cycle 24 (with monthly sunspot number of 1.2). They correspond to the minimum and the maximum GCR proton fluxes in the time range from 1995 and 2020.

Proton spectra during peak 2 hours of considered SEP events measured between 1995 and 2015 outside Earth's magnetosphere [20] by the Solar and Heliospheric Observatory (SOHO) are shown in Fig.1 by straight lines (and enveloped in the shaded area). These SEP events all have protons with energies greater than 500 MeV and a single power law is assumed to reconstruct each spectrum in the energy range of 50 and 800 MeV from the measurement. Note that the flux is not a direct measurement, but derived using an inversion process. In reality, these SEP spectra may extend to a larger or smaller energy range and have a different spectral shape (such as a double power-law distribution). In this study, the SEP spectra are assumed to extend between 10 MeV and 1 GeV as input for the REDEarth model.

Figure 2 shows altitude- and energy-dependence of primary protons and induced neutrons for GCRs during solar min (left panels) and a strong SEP with a hard spectrum which occurred on November 5, 2003, right panels). The influence of Earth's magnetic field, which will be discussed later, is not accounted for in this plot, so the results should be considered to represent particle fluxes above the magnetic poles of the Earth. Since the energy axis is logarithmic, we present the spectrum in units of lethargy. In this way, the energy spectral shape looks more similar to a regular differential flux with energy in linear scale. It can be seen that primary GCR protons (panel a) have higher energies and can penetrate to lower altitudes compared to SEP protons (panel c). However, neither primary GCR nor SEP protons can reach altitudes lower than 10 km. Radiation field at these altitudes is dominated by secondary radiation, mainly neutrons (panel b and d). Neutron flux reaches a peak between 10-30km altitude, where the total vertical column depth of the atmosphere is about 150 g/cm^2 (for 20km altitude). Since GCRs comprise protons with the energy much higher than those in SEPs, the peak (panel b) is shifted to slightly lower altitudes for GCRs than for SEPs (panel d). The difference in flux intensity is more significant: During the peak phase of the SEP event, associated neutron fluxes are much higher than that of background GCRs. Note that the resonance features in neutron spectra (seen as vertical bright lines around a few MeV) are similar for GCR and SEP induced neutrons.

In addition, we also need to consider the geomagnetic shielding of the primary charged particles. The ability of charged particles to pass through the magnetosphere depends

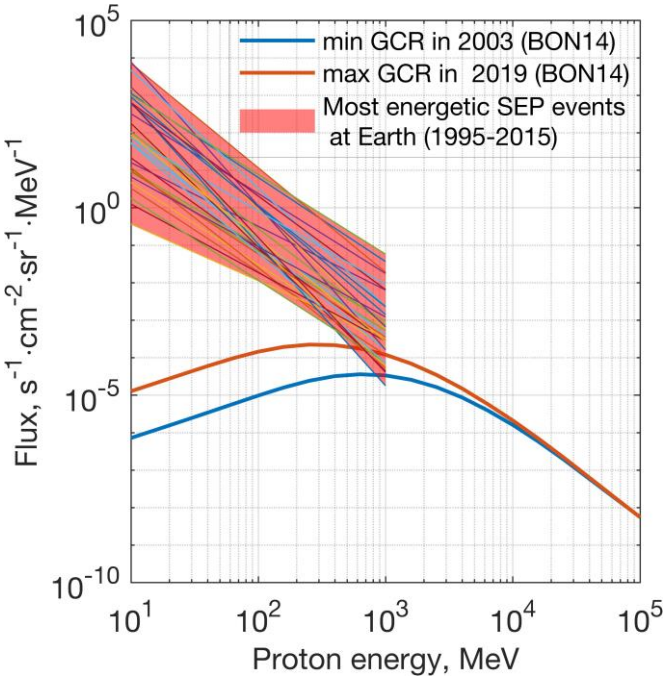

Fig. 1: Energy spectra of proton flux at various radiation conditions, including GCR proton spectra during 2003 (maximum of Solar cycle 23) and 2019 (minimum of Solar cycle 24) and the derived power-law spectra of 32 SEP events with proton energy extending above 500 MeV detected between 1995 and 2015 as derived by [20].

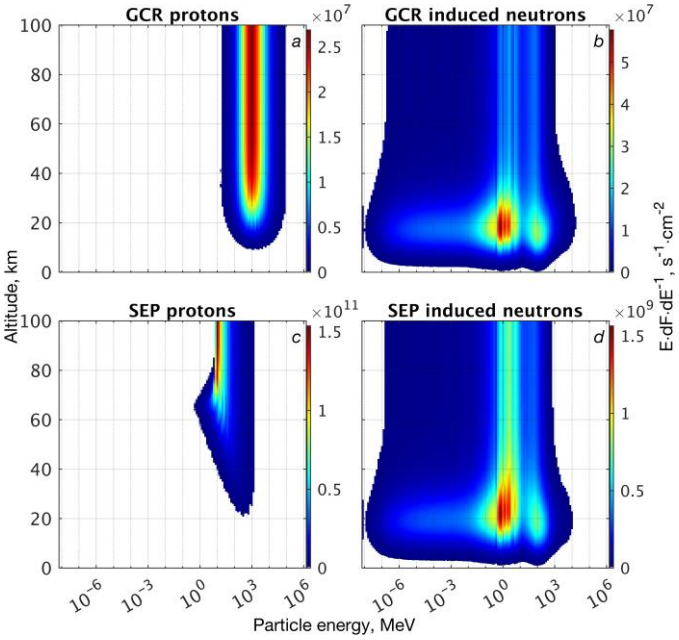

Fig. 2: Altitude profiles of GCR and SEP proton spectra per lethargy ($E \cdot dF\ (E)/dE$) and their induced neutron spectra calculated with the REDEarth model. The difference in the flux intensity does not show well when using one scale for all panels, so each panel has its own color scale.

on the zenith and azimuth angle of particle's momentum and particle's rigidity. However, the description of the ability of a particle to pass through the magnetosphere as a function of its incoming direction is rather complicated and the geomagnetic cut-off is often characterized with EVGCR which averages out the incoming angles. EVGCR is strongest in the region of Southeast Asia and weakest near the magnetic poles. Geomagnetic cutoff rigidities at few locations based on data in [13] are shown in Table.I. These EVGCR values are applied to the primary particle spectra (Fig.1) before we model the particle interaction in the Earth's atmosphere with REDEarth.

TABLE I: Values of effective vertical geomagnetic cut-off rigidity (EVGCR) at selected locations

Geographic location	EVGCR (GV)
Anchorage	0.98
Johannesburg	1.9
New York	1.9
Washington	2.2
London	3.1
Sydney	4.9
Miami	5.3
Tokyo	12.0

In Figure 3 we show REDEarth prediction of neutron fluence versus experimental measurements at 20 km altitude with 0.8 GV EVGCR during July 1997. Due to the unpredictable nature of SEP events that limits the experimental planning, this validation is carried out against background GCR measurement by [14]. Despite overestimation of the experimental data in below energy of ∼1 MeV, the REDEarth model predictions are in a good agreement with the experimental data. Neutrons below 1 MeV are more sensitive to atmospheric humidity and density fluctuations. Also, for aviation electronics influence of neutrons with energy above 1 MeV is much more significant, compared to neutrons with lower energy. The difference in neutron flux at energies above 1 GeV might result from sensitivity of the detectors used in the experiment.

IEC 62396 standard considers only neutron intensity of sufficient energy as capable to impart damaging charges and result in SEB. Hence a minimum cut-off energy of $> 10MeV$ for neutron flux is applied.

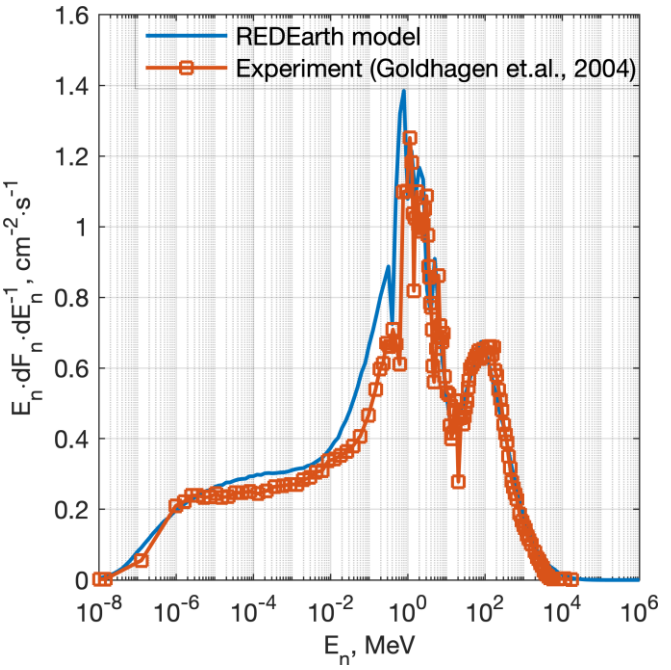

Fig. 3: Experimental and calculated differential energy spectra per lethargy ($E \cdot dF\ (E)/dE$) of neutrons at 20 km altitude altitude for averaged GCR conditions in July 1997.

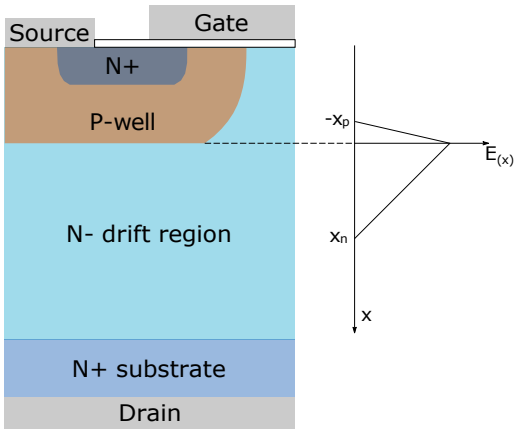

Fig. 4: SiC MOSFET Cross section and internal electric field in blocking mode

III. CR-INDUCED FAILURE RATES PREDICTION USING REVISED DATA

A. Experimentally measured CR-induced failure rate

CR-induced failures are dependent on the breakdown voltage rating of the device, the applied voltage and consequent device internal electric field during blocking period along with the CR intensity. Fig. 4 shows a possible electric field distribution of a vertical power MOSFET [22].

Modeling of SEB phenomenon is a complex multi physics problem [8], [23]. The approved method is to experimentally measure failure rates at multiple reverse bias voltages and extrapolate the failure rate based on the variation in radiation intensity. A study considering few different device types was reported in [24] at different voltage ratings. A more recent research effort at Los Alamos analyzed SiC devices from various vendors and was able to identify a universal trend for CR induced failure rate [25]. The identified universal trend corroborates well with previous research efforts in quantifying CR induced failure rates.

Typical workflow for CR induced failure rate estimation is summarized in Fig. 5. Fig.6 summarizes the variation in CR flux of interest for SEB calculation. The units of flux is per cm^2/h.The reference flux at New York at sea level is 12.6 neutrons per cm^2/h.

A key observation to be made from the above figure is that the high energy particle flux that result in SEBs are higher than the IEC recommended values. During Solar events, the SEB inducing flux increases to a much higher value necessitating mitigation measures such as voltage modulation proposed in

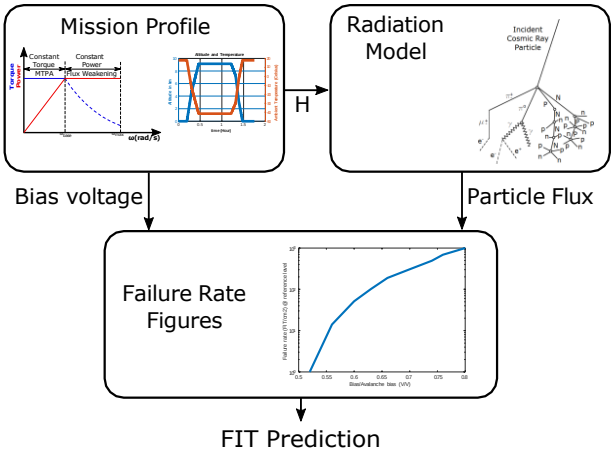

Fig. 5: CR-induced failure rate estimation flowchart

[12] or thermal control proposed in [26]. GCR minimum flux is more conservative steady state value for assessing impact of CRs on lifetime reliability.

IV. Case Study of Starter Generator System

The accurate modeling of the radiation profile together with physics-of failure reliability models will be used in this section to show how this work can be used for both hazard prediction and mitigation.

Several strategies are available to mitigate against CR-induced failures. One of the earliest recommendations from the IEC 62396 standards committee was to de-rate the power semiconductors for aviation to 50% [27]. An analytical expression for CR-induced failure, given in Eq.(1), was proposed by ABB for a particular class of power modules that is voltage dependent [28]. The temperature dependency of the CR-induced failure rate was found to be a material specific property. This phenomenon can be explained due to the increase in mean free path for charge carriers at lower temperatures. Another mechanism of failure in Si devices is turn-on of the parasitic bi-polar junction transistor which is not prevalent in SiC devices. The chance of a streamer formation due to CR is higher at lower temperatures. The increase in mean free path at lower temperatures manifests as a reduction in breakdown voltage of semiconductors. The breakdown voltage relationship with temperature has been presented in literature [29].

$$\lambda\left(V_{DC}, T_j, h\right) = C_3 \cdot \exp\left(\frac{C_2}{C_1}\right)^{V_{DC}} \cdot \exp\left(\frac{25 - T_j}{47.6}\right) \cdot \exp\left(\frac{1 - \left(1 - \frac{h}{44300}\right)^{5.26}}{0.143}\right) \quad (1)$$

The coefficients in Eq.1 are summarized below:

- C_1, C_2 and C_3 account for device specific characteristics and blocking voltage. These parameters have no physical meaning as they are derived by curve fitting. The unit of V_{DC} is in volts. The equation is only valid for V_{DC} greater than C_1. The failure rate is regarded as zero otherwise.
- T_j is the junction temperature in degree Celsius.
- h is the height in meters above sea level.

The effect of temperature on failure rate is a material specific property of the semiconductor and is uniform across devices made from the same material. Altitude accounts for the variation in CR intensity and is device/material independent.

Based on equation 1, voltage de-rating and thermal control are two options to reduce CR-induced failure rate. Unlike static de-rating during design phase, dynamic voltage variation was proposed [12] during high solar activity as a mitigation measure. Furthermore, solar events tend to last for short duration of 2-3 days and the peak lasts for few hours [30]. Hence these mitigation actions are only active for short duration and there is minimal impact on long term reliability of the converter systems. In this section, the impact of dynamic voltage variation on system performance is presented.

A. Starter Generator System

Starter generators are used in aircraft to spin up the main turbine from stand-still without external systems [31]. After the main turbine has achieved operational speed, the system mode is changed to generation to feed the aircraft electrical network. A schematic of a 2L-SiC based drive system is shown in Fig. 7. This drive arrangement can operate in generation or drive mode (bi-directional).

The nominal parameters of the electrical machine used as a case study and the Drive are summarized in Table. II. Based on the machine parameters, flux weakening is necessary below DC link voltage of 700V to keep maintain nominal output power.

TABLE II: Starter generator parameters

Nominal Power	30 kW
Phase and pole numbers	3 phase, 6 poles
Nominal mechanical speed	12000 rpm
Stator resistance	1.1 mΩ
Ld (d-axis inductance)	250 μH
Lq (q-axis inductance)	350 μH
Back EMF constant, Ke	0.1065 V · s/rad

The drive converter parameters are summarized in Table. III.

TABLE III: Drive parameters

Nominal DC Link, Vdc	840 V
SiC Device	CAB016M12FM3
Device Rating	1200V,78A
Thermal Resistance [Case to Ambient]	0.2 K/W
Ambient Temperature	50 degC
Switching Frequency	40 kHz
DC Link Capacitance	400 μF
Capacitor ESR	5 mΩ

B. Simulation of Starter Generator System

The system parameters at various DC link voltages from 600V to 900V with 30V granularity is simulated to evaluate

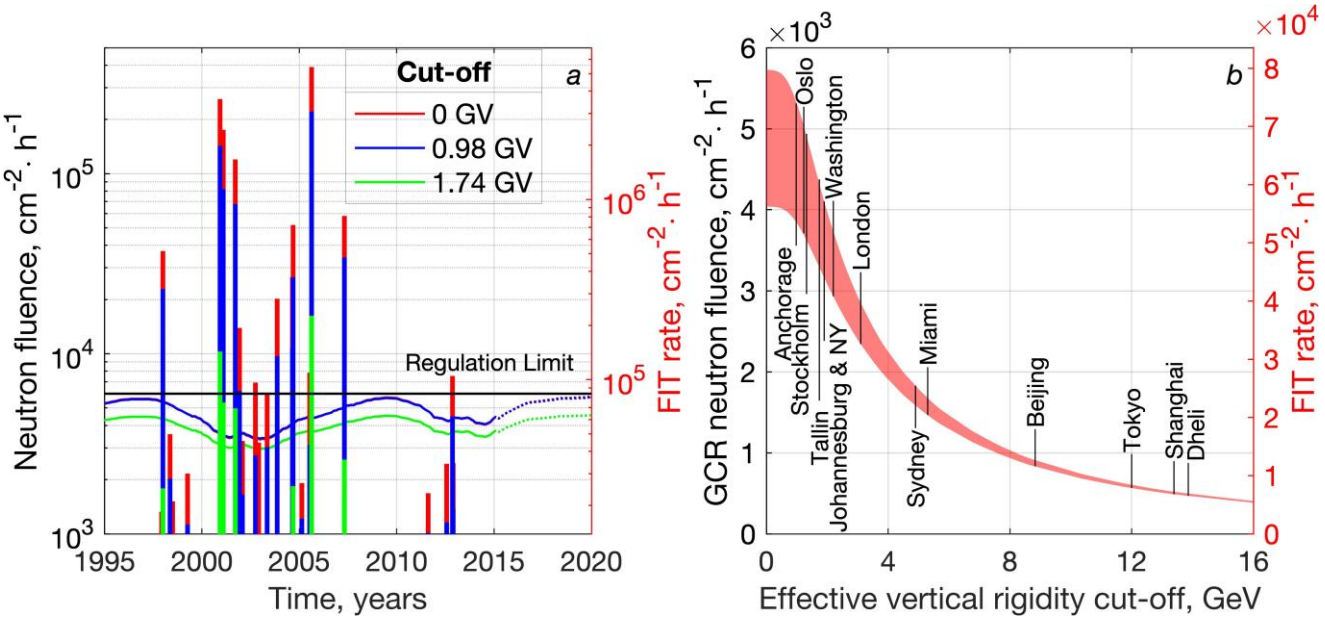

Fig. 6: a) SEB inducing neutron flux at 10km altitude due to various SEP events (bars) between 1995 and 2015 and the time-dependent background GCR flux (curves) between 1995 and 2020. Different colors denote the results of different cutoff rigidity which is related to the geographical location. Dotted line shows time interval where no SEP data is included. b) The SEB inducing neutron flux contributed by background GCRs at different geographical locations during solar maximum (lower bound of the shaded area) and minimum (upper bound) conditions.

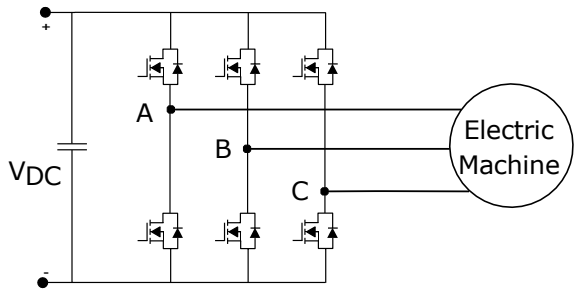

Fig. 7: Starter Generator Drive Schematic

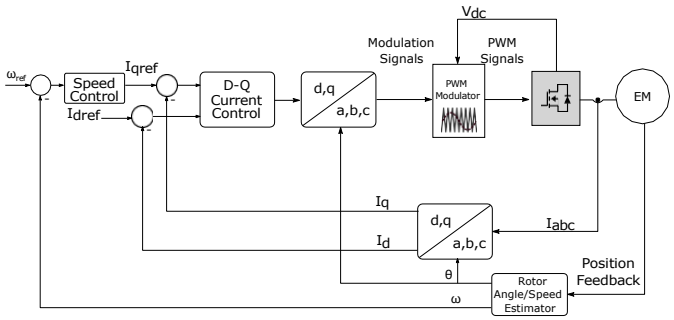

Fig. 8: Starter Generator Drive Control Structure, starting mode.

the impact on drive converter stresses against CR mitigation benefit. The key stresses considered are semiconductor losses and capacitor losses. SiC MOSFETs are bidirectional devices and hence diode losses are not considered. The switching losses are calculated by scaling the reference turn-on and turn-off loss figures from data-sheet with the simulated turn-on and turn-off currents during a fundamental electrical cycle. The control structure for the drive converter is shown in Fig. 8. The power electronics is configured with a speed loop in the starting mode, and then switches to voltage control mode (Fig. 13) once the main engine is ignited. Inner current control follows the vector control paradigm as outlined in [32], [33].

In order to bring out the relative variation of losses, thermal stresses and CR-induced failure rate, normalized plots are provided in the simulated DC link voltage range. The nominal values at reference operating condition of 840V DC link is provided in Table. IV.

The variation of switching and conduction losses as well as overall converter losses including capacitor ESR losses are shown in Fig. 9. The variation in switching in conduction losses can be attributed to the machine winding currents as well as the DC link variation. The machine winding current variation and DC power output is shown in Fig. 10.

TABLE IV: Drive Nominal Values

Vdc	840 V
Torque	-24.5 Nm
Power	30.6 kW
Switching Losses	69.4 W
Conduction Losses	100.8 W
Capacitor Losses	1.9 W
Junction Temperature	99.99 degC
Winding Current	51.15A
FIT Rate	175.4 /cm2
CR Temperature Coefficient	0.21

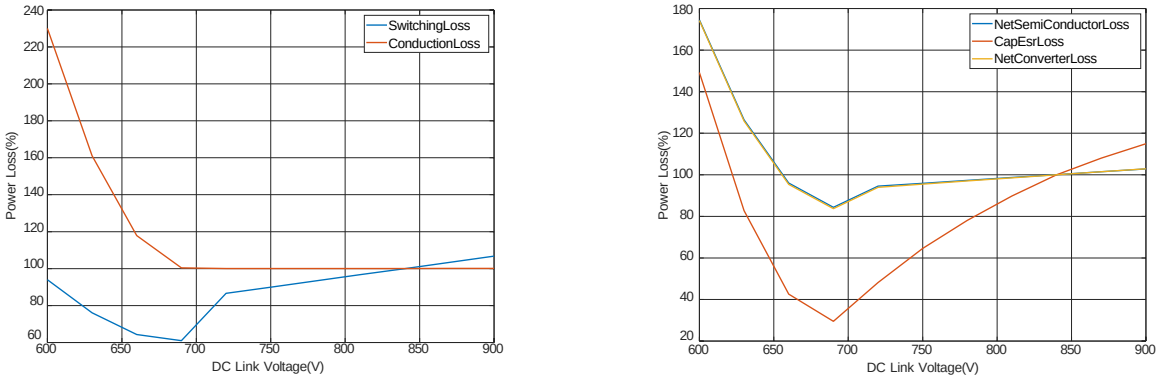

(a) Semiconductor Loss Profile (b) Converter loss profile

Fig. 9: Drive system loss variation with DC link Voltage

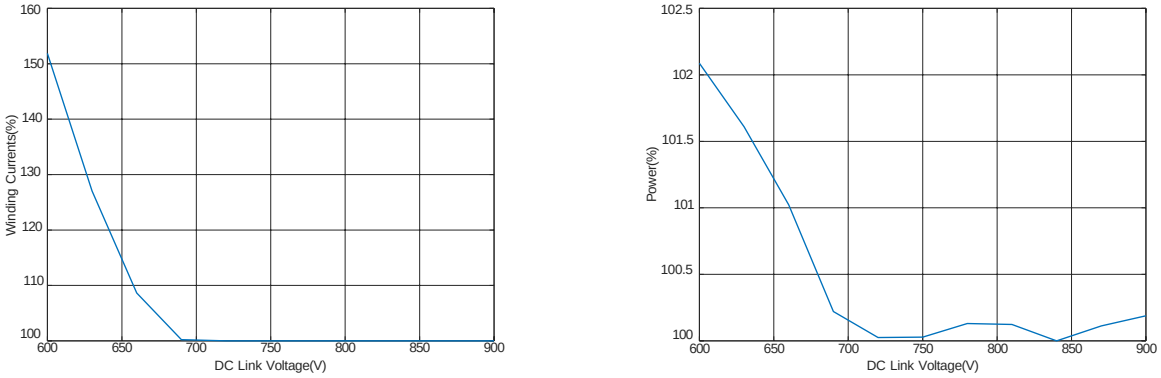

(a) Semiconductor Loss Profile (b) Converter loss profile

Fig. 10: Drive system loss variation with DC link Voltage

Applying the trend identified in [25] for SiC CR-induced failure rate, the following trend is obtained for device FIT rate under DC link variation Fig. 11. More than 20 times reduction in CR FIT rate can be achieved by reducing the DC link from 840V to 700V which is a significant mitigation option during high Solar activity.

DC link voltage variation impacts the losses in the drive system. The impact of this on semiconductor junction temperature is extracted and shown in Fig. 12. This information is necessary to assure operating within device safe operation limits.

DC link voltage control is controlled by the upstream converters which interface to energy sources - generators, batteries etc. A typical control structure for a generator interfaced control with cosmic ray mitigation control integrated is shown in Fig. 13. In generator mode, the drive operates as voltage control and the active reliability control defines the voltage reference.

As shown in Eq. (1), there is an inverse relationship between CR-induced failure rate and device temperature. Thus, higher device losses provide an additional reduction in CR FIT rate. The nominal CR-induced failure rate temperature coefficient

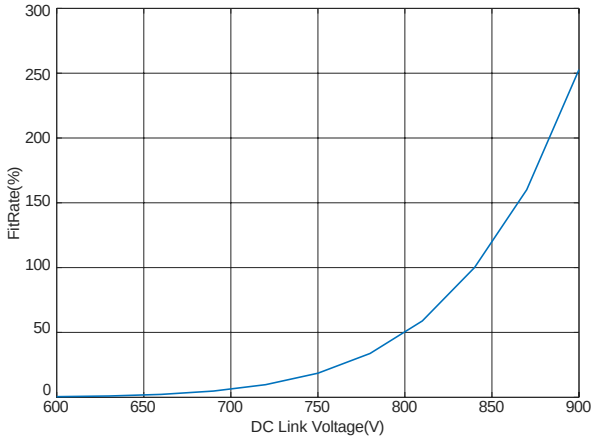

Fig. 11: Normalized FIT rate of SiC devices at various DC link voltages

shown in Table. IV shows a reduction of 20% from reference failure rate at 25°C . In Fig. 14, normalized temperature coefficients of CR-induced failure rate shows that at lower

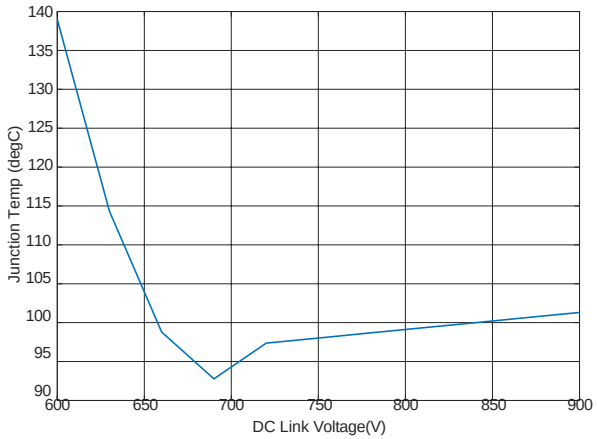

Fig. 12: Junction temperature of semiconductors under various DC link voltages

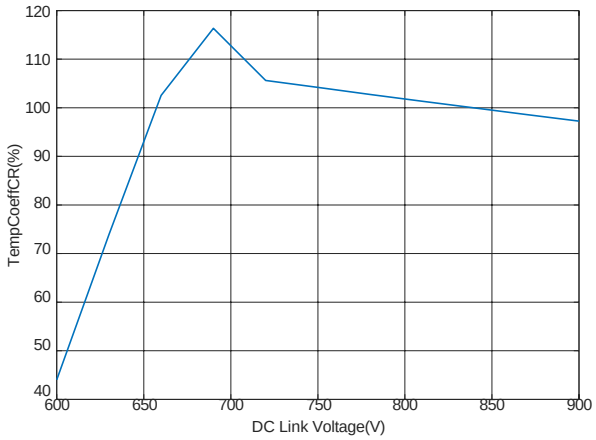

Fig. 14: Normalized CR-induced failure rate Temperature Coefficient

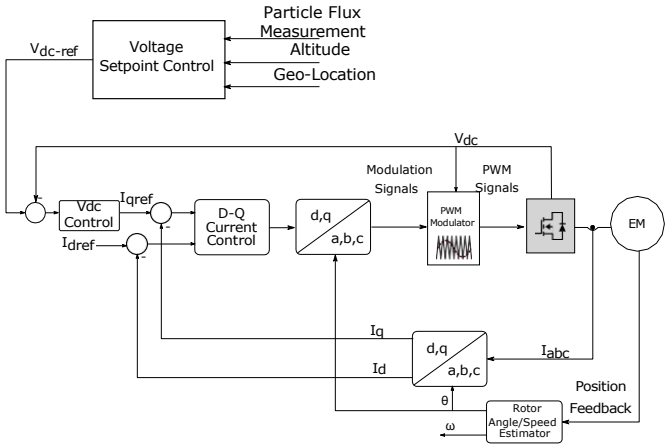

Fig. 13: Generator Control Structure with real-time voltage de-rating.

DC link voltages, we get an additional reduction in CR-induced failure rate. It must be noted that the temperature dependence for Si IGBT devices is presented in Eq. (1). The same relationship has been applied to SiC devices in this work as studies showing temperature dependence of cosmic ray failure rates for SiC devices are not available in literature yet. Leakage current increase with increase in temperature have been noted under particle irradiation of SiC mosfets [34]. However more studies are required to establish temperature dependence of SEB in SiC devices.

V. Conclusion

This study has analyzed the effects of the CRs both in the case of background GCR radiation and during strong solar events. Particle spectra reconstructed from models and measurements are used as an input for REDEarth model that is used to evaluate the particle flux at a given cruise altitude at different geographical locations around the world. The objective is to evaluate the risk of single-event-background radiation on power electronics on-board the aircraft. We conclude that the radiation flux recommended by IEC standard is appropriate for static de-rating design in high reliability applications, but the risk of failure during SEP storms vastly exceeds the standard, calling for mitigation actions. Furthermore, the effectiveness of voltage control during solar events show that voltage de-rating is a suitable mitigation measure against CR-induced failures.

References

[1] V. Madonna, P. Giangrande, and M. Galea, "Electrical power generation in aircraft: Review, challenges, and opportunities," *IEEE Transactions on Transportation Electrification*, vol. 4, no. 3, pp. 646–659, Sep. 2018.

[2] G. Buticchi, P. Wheeler, and D. Boroyevich, "The more-electric aircraft and beyond," *Proceedings of the IEEE*, pp. 1–15, 2022.

[3] C. M. Cohen, G. Li, G. M. Mason, A. Y. Shih, and L. Wang, *Solar Energetic Particles*, 2021, vol. 5.

[4] J. Simpson, "Elemental and isotopic composition of the galactic cosmic rays," *Annual Review of Nuclear and Particle Science*, vol. 33, no. 1, pp. 323–382, 1983.

[5] H. Cane, G. Wibberenz, I. Richardson, and T. Von Rosenvinge, "Cosmic ray modulation and the solar magnetic field," *Geophysical Research Letters*, vol. 26, no. 5, pp. 565–568, 1999.

[6] M. Kallenrode, "Current views on impulsive and gradual solar energetic particle events," *Journal of Physics G: Nuclear and Particle Physics*, vol. 29, no. 5, p. 965, 2003.

[7] *Process management for avionics — Atmospheric radiation effects*, International Electrotechnical Commission, 2017.

[8] G. Soelkner, "Ensuring the reliability of power electronic devices with regard to terrestrial cosmic radiation," *Microelectronics Reliability*, vol. 58, pp. 39 – 50, 2016, reliability Issues in Power Electronics. [Online]. Available: http://www.sciencedirect.com/science/article/pii/S0026271415302663

[9] D. U. Schilling, *Cosmic Ray Failures in Power Electronics*, Semikron Gmbh, Jun. 2017.

[10] B. Smet, "An empiric approach to establishing mosfet failure rate induced by single-event burnout," in *2008 13th International Power Electronics and Motion Control Conference*, 2008, pp. 102–107.

[11] M. I. Dobynde, S. I. Svertilov, and M. I. Panasyuk, "Calculating the Radiation Dose Rates Created by Cosmic Rays in the Earth ' s Atmosphere," vol. 85, no. 11, pp. 1642–1645, 2021.

[12] J. Guo, G. Buticchi, and C. Gerada, "Space weather prediction to enhance the reliability of the more electric aircraft," in *2018 IEEE 27th International Symposium on Industrial Electronics (ISIE)*, 2018, pp. 445–450.

[13] J. F. Ziegler, "Terrestrial cosmic rays," *IBM Journal of Research and Development*, vol. 40, no. 1, pp. 19–39, Jan 1996.

[14] P. Goldhagen, J. M. Clem, and J. W. Wilson, "The energy spectrum of cosmic-ray induced neutrons measured on an airplane over a wide range of altitude and latitude," *Radiation Protection Dosimetry*, vol. 110, no. 1-4, pp. 387–392, 08 2004. [Online]. Available: https://doi.org/10.1093/rpd/nch216

[15] C. J. Mertens, M. M. Meier, S. Brown, R. B. Norman, and X. Xu, "NAIRAS aircraft radiation model development, dose climatology, and initial validation," *Space Weather*, vol. 11, no. 10, pp. 603–635, 2013.

[16] J. Guo, S. Banjac, L. Ro¨stel, J. C. Terasa, K. Herbst, B. Heber, and R. F. Wimmer-Schweingruber, "Implementation and validation of the GEANT4/AtRIS code to model the radiation environment at Mars," *Journal of Space Weather and Space Climate*, vol. 9, no. A2, 2019.

[17] M. I. Dobynde and J. Guo, "Radiation environment at the surface and subsurface of the moon: Model development and validation," *Journal of Geophysical Research: Planets*, vol. 126, no. 11, p. e2021JE006930, 2021.

[18] S. Agostinelli, J. Allison, K. Amako, J. Apostolakis, H. Araujo, P. Arce, M. Asai, D. Axen, S. Banerjee, G. Barrand *et al.*, "GEANT4: a simulation toolkit," *Nuclear Instruments and Methods in Physics Research Section A*, vol. 506, no. 3, pp. 250–303, 2003.

[19] *U.S. Standard Atmosphere, 1976*, 1976.

[20] P. Ku¨hl, N. Dresing, B. Heber, and A. Klassen, "Solar Energetic Particle Events with Protons Above 500 MeV Between 1995 and 2015 Measured with SOHO/EPHIN," *Solar Physics*, vol. 292, no. 1, 2017. [Online]. Available: http://dx.doi.org/10.1007/s11207-016-1033-8

[21] P. O'Neill, S. Golge, and T. Slaba, "Badhwar–O'Neill 2014 Galactic Cosmic Ray Flux Model," *NASA/TP*, vol. 218569, 2015. [Online]. Available: https://ntrs.nasa.gov/archive/nasa/casi.ntrs.nasa.gov/20150003026.pdf

[22] H. Qin, Y. Mo, Q. Xun, Y. Zhang, and Y. Dong, "A digital-controlled sic-based solid state circuit breaker with soft switch-off method for dc power system," *Electronics*, vol. 8, no. 8, 2019. [Online]. Available: https://www.mdpi.com/2079-9292/8/8/837

[23] T. Shoji, S. Nishida, K. Hamada, and H. Tadano, "Experimental and simulation studies of neutron-induced single-event burnout in sic power diodes," *Japanese Journal of Applied Physics*, vol. 53, no. 4S, p. 04EP03, feb 2014. [Online]. Available: https://dx.doi.org/10.7567/JJAP.53.04EP03

[24] C. Felgemacher, S. V. Arau´jo, P. Zacharias, K. Nesemann, and A. Gruber, "Cosmic radiation ruggedness of si and sic power semiconductors," in *2016 28th International Symposium on Power Semiconductor Devices and ICs (ISPSD)*, June 2016, pp. 51–54.

[25] A. Akturk, J. M. McGarrity, N. Goldsman, D. J. Lichtenwalner, B. Hull, D. Grider, and R. Wilkins, "Predicting cosmic ray-induced failures in silicon carbide power devices," *IEEE Transactions on Nuclear Science*, vol. 66, no. 7, pp. 1828–1832, 2019.

[26] J. Harikumaran, G. Buticchi, G. MIgliazza, P. Wheeler, and M. Galea, "Reliability oriented thermal management of aircraft power converters," in *2020 IEEE 9th International Power Electronics and Motion Control Conference (IPEMC2020-ECCE Asia)*, 2020, pp. 1590–1594.

[27] R. Edwards, "Technical specification foratntospheric radiation single event effects (see) on avionics electronics," Goodrich, 2005.

[28] N. Kaminski, *Failure Rates of HiPak Modules Due to Cosmic Rays Application Note 5SYA 2042-02*, ABB Switzerland Ltd, 2004.

[29] R. Rupp, R. Gerlach, A. Kabakow, R. Scho¨rner, C. Hecht, R. Elpelt, and M. Draghici, "Avalanche behaviour and its temperature dependence of commercial sic mps diodes: Influence of design and voltage class," in *2014 IEEE 26th International Symposium on Power Semiconductor Devices and IC's (ISPSD)*, 2014, pp. 67–70.

[30] M. Laurenza, G. Consolini, M. Storini, and A. Damiani, "A shannon entropy approach to the temporal evolution of sep energy spectrum," *Astrophysics and Space Sciences Transactions*, vol. 8, 02 2012.

[31] S. Bozhko, T. Yang, J. Le Peuvedic, P. Arumugam, M. Degano, A. La Rocca, Z. Xu, M. Rashed, W. Fernando, C. I. Hill, C. Eastwick, S. Pickering, C. Gerada, and P. Wheeler, "Development of aircraft electric starter–generator system based on active rectification technology," *IEEE Transactions on Transportation Electrification*, vol. 4, no. 4, pp. 985–996, Dec 2018.

[32] S.-H. Kim, "Chapter 5 - vector control of alternating current motors," in *Electric Motor Control*, S.-H. Kim, Ed. Elsevier, 2017, pp. 203–246. [Online]. Available: https://www.sciencedirect.com/science/article/pii/B9780128121382000052

[33] D. G. Holmes and T. A. Lipo, *Frontmatter*. Wiley-IEEE Press, 2003, pp. 744–. [Online]. Available: https://ieeexplore.ieee.org/xpl/articleDetails.jsp?arnumber=5312026

[34] S. A. Ikpe, J.-M. Lauenstein, G. A. Carr, D. Hunter, L. L. Ludwig, W. Wood, C. J. Iannello, L. Y. Del Castillo, F. D. Fitzpatrick, M. M. Mojarradi, and Y. Chen, "Long-term reliability of a hard-switched boost power processing unit utilizing sic power mosfets," in *2016 IEEE International Reliability Physics Symposium (IRPS)*, 2016, pp. ES–1–1–ES–1–8.